

Contents lists available at ScienceDirect

Water Research

journal homepage: www.elsevier.com/locate/watres





Antiscalants for mitigating silica scaling in membrane desalination: Effects of molecular structure and membrane process

Yiqun Yao, Xijia Ge, Yiming Yin, Ronny Minjarez, Tiezheng Tong

Department of Civil and Environmental Engineering, Colorado State University, Fort Collins, CO 80523, United States

ARTICLE INFO

Keywords: Silica scaling Antiscalants Membrane distillation Reverse osmosis

ABSTRACT

Silica scaling is a major type of mineral scaling that significantly constrains the performance and efficiency of membrane desalination. While antiscalants have been commonly used to control mineral scaling formed via crystallization, there is a lack of antiscalants for silica scaling due to its unique formation mechanism of polymerization. In this study, we performed a systematic study that investigated and compared antiscalants with different functional groups and molecular weights for mitigating silica scaling in membrane distillation (MD) and reverse osmosis (RO). The efficiencies of these antiscalants were tested in both static experiments (for hindering silicic acid polymerization) as well as crossflow, dynamic MD and RO experiments (for reducing water flux decline). Our results show that antiscalants enriched with strong H-accepters and H-donors were both able to hinder silicic acid polymerization efficiently in static experiments, with their antiscaling performance being a function of both molecular functionality and weight. Although poly(ethylene glycol) (PEG) with abundant Haccepters exhibited high antiscaling efficiencies during static experiments, it displayed limited performance of mitigating silica scaling during MD and RO. Poly (ethylene glycol) diamine (PEGD), which has a PEG backbone but is terminated by two amino groups, was efficient to both hinder silicic acid polymerization and reduce water flux decline in MD and RO. Antiscalants enriched with H-donors, such as poly(ethylenimine) (PEI) and poly (amidoamine) (PAMAM), were effective of extending the water recovery of MD but conversely facilitated water flux decline of RO in the presence of supersaturated silica. Further analyses of silica scales formed on the membrane surfaces confirmed that the antiscalants interacted with silica via hydrogen bonding and showed that the presence of antiscalants governed the silica morphology. Our work indicates that discrepancy in antiscalant efficiency exists between static experiments and dynamic membrane filtration as well as between different membrane processes associated with silica scaling, providing valuable insights on the design principle and mechanisms of antiscalants tailored to silica scaling.

1. Introduction

Water is an essential resource for human activities and ecosystem health (Grant et al., 2012), but our society is facing dual challenges of water pollution and scarcity due to the rapid growth of population and a changing climate (Hoekstra, 2014; Vörösmarty et al., 2010), Membrane-based desalination and wastewater treatment have attracted tremendous attention as a promising approach that enables water purification from a variety of unconventional sources including seawater, brackish water, and wastewater (Charcosset, 2009). However, the performance and efficiency of membrane technologies are significantly constrained by mineral scaling, a prominent problem caused by the existence of scale precursors that form sparingly soluble minerals (Rolf

et al., 2022; Tong et al., 2019a, 2019b; Warsinger et al., 2015). The formation and/or deposition of mineral scales on the membrane surface decreases water flux (i.e., water productivity) and the membrane lifespan, thereby increasing the cost, energy consumption, and carbon footprint of membrane desalination and treatment (Rolf et al., 2022; Tong et al., 2019b).

Mineral scales can be generated via two distinct mechanisms: crystallization and polymerization. The former leads to the formation of crystalline minerals such as gypsum and calcite (Tong et al., 2019b). while the latter is unique for the occurrence of amorphous silica scale (Wallace et al., 2009). Compared to gypsum and calcite scaling, silica scaling is more challenging to deal with, largely due to the lack of efficient antiscalants. For example, phosphonate- and carboxylic-based

E-mail address: tiezheng.tong@colostate.edu (T. Tong).

^{*} Corresponding author.

have shown effectively antiscalants been to crystallization-induced gypsum and calcite scaling during membrane desalination (Chaussemier et al., 2015; He et al., 2009; Reiss et al., 2020; Turek et al., 2017; Warsinger et al., 2015; Yin et al., 2021; Yu et al., 2020). However, only a few publications have attempted to develop antiscalants that are able to hinder silica polymerization (Demadis and Neofotistou, 2007; Neofotistou and Demadis, 2004; Preari et al., 2014), and these studies are dominantly based on results from static experiments without the presence of a membrane. Recently, we reported that mitigating gypsum scaling and silica scaling in membrane distillation (MD) requires antiscalants with distinct molecular functionalities (Yin et al., 2021). Antiscalants possessing Ca(II)-complexing moieties (e.g., carboxyl group) exhibited the best efficiencil of inhibiting gypsum scaling, whereas antiscalants enriched with amino groups were the most effective to mitigate silica scaling (Yin et al., 2021). Although our work demonstrates the possibility of developing antiscalants that are able to reduce silica scaling in crossflow, dynamic membrane desalination, an in-depth understanding of the design criteria and mechanisms for antiscalants tailored to silica scaling has yet to be established.

Furthermore, different membrane processes have been applied to the treatment of feedwaters with varied salinities. Reverse osmosis (RO) is the most energy efficient desalination technology where thin-film composite (TFC) polyamide membranes are used to selectively separate water from salts with high efficiency (Elimelech and Phillip, 2011; Lu and Elimelech, 2021). Depsite its advantages, RO is contrained by its salinity limit (typically 70,000 mg/L) (Tong and Elimelech, 2016), which is due to the maximum hydraulic pressure tolerable by current membrane modules. Hence, other membrane technologies such as MD have emerged to desalinate hypersaline brines possessing salinities beyond the RO limit (Shaffer et al., 2013; Tong and Elimelech, 2016). As a thermal-membrane hybrid process, MD enables desalination by utilizing a vapor pressure difference that drives water transport across a microporous, hydrophobic membrane (Atia et al., 2021; Deshmukh et al., 2018; Tong et al., 2019a). This technology is theoretically capable of concentrating brines to up to >200,000 mg/L (Tong and Elimelech, 2016), with its capability of utilizing low-grade thermal energy providing additional benefits of reducing the cost and carbon footprint of hypersaline brine treatment (Deshmukh et al., 2018). The differences in membrane material and feedwater salinty between RO and MD might result in different membrane scaling behaviors and mechanisms. While dense, "non-porous" polyamide membranes have been typically used in RO (Elimelech and Phillip, 2011; Lu and Elimelech, 2021), MD empolys hydrophobic membranes with larger pore sizes at the micron scale (Deshmukh et al., 2018). Compared to MD, RO is employed to desalinate feedwaters with lower salinities (and correspondingly lower concentrations of scale-forming species). Those differences between MD and RO potentially lead to distinct design and working principles of

antiscalants. However, no studies have been reported to compare the behaviors and efficiencies of antiscalants between MD and RO.

In this work, we performed a systematic study that investigated and compared the efficiencies of antiscalants with different molecular structures for mitigating silica scaling in MD and RO. We selected several groups of candidate antiscalants with distinct functional groups (Fig. 1). As existing studies have shown the importance of hydrogen bonding in the silica-organic interactions (Kempter et al., 2013; Preari et al., 2014), the selected antiscalants possess varied capabilities of forming hydrogen bond. Poly(ethylene glycol) (PEG) represents a group of uncharged organic molecules with functional groups as H-accepters (i.e., the ethereal oxygens) (Malmsten et al., 1992; Preari et al., 2014; Rubio and Kitchener, 1976), while organic molecules such as poly (ethylenimine) (PEI), poly(amidoamine) (PAMAM), and polyvinyl alcohol (PVA), were selected to represent antiscalants with abundant functional groups as strong (e.g., primary and secondary amine groups) (Kröger et al., 2000; Mizutani et al., 1998) and moderate (e.g., hydroxyl group) H-donors (Pike et al., 2019), respectively. Antiscalants with different molecular weights (MW) were also used to investigate the effect of molecular size on their anti-scaling efficacy. The efficiencies of these antiscalants were tested during both static experiments (for hindering silica polymerization) as well as crossflow, dynamic MD and RO experiments (for reducing water flux decline caused by silica scaling). By doing so, we are able to answer three key questions associated with antiscalants for silica scaling: (1) how the performance of antiscalants behave as a function of molecular functionality and weight; (2) whether the efficiencies of antiscalants revealed from static experiments are able to predict those in crossflow, dynamic membrane filtration; and (3) whether MD and RO require antiscalants with the same molecular functionality. In addition, we analyzed the morphologies and binding chemistry of silica scales formed on the membrane surfaces in the presence of different antiscalants to reveal the silica-antiscalants interactions, which provide insights on the potential antiscaling mechanisms.

2. Materials and methods

2.1. Materials and chemicals

Sodium metasilicate pentahydrate ($Na_2SiO_3 \cdot 5H_2O$), sodium bicarbonate ($NaHCO_3$), ammonium molybdate tetrahydrate ((NA_4)₆Mo₇O₂₄·4H₂O), and oxalic acid dihydrate ($C_2H_2O_4 \cdot 2H_2O$) were provided by Sigma-Aldrich (St. Louis, MO). Sodium chloride (NaCl), sodium hydroxide (NaOH), and hydrochloric acid (HCl) were purchased from Fisher Chemicals (Hampton, NH). PEG with MW of 1500, 3000, 6000, 10,000, and 20,000, PEGD with MW of 10,000, PVA with MW of 13,000, 27,000 and 61,000, branched PEI with MW of 800 and 10,000,

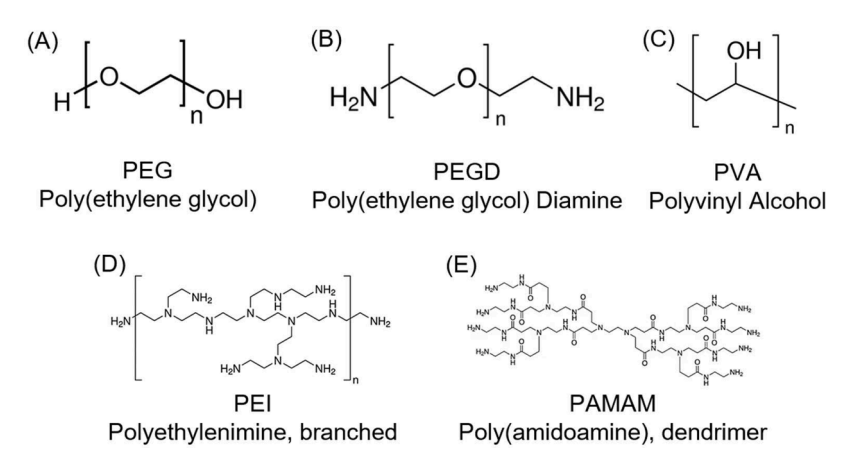


Fig. 1. Chemical structures of candidate antiscalants for (A) PEG, (B) PEGD, (C) PVA, (D) PEI, and (E) PAMAM.

and PAMAM dendrimers with MW of 1430 (all purchased from Sigma-Aldrich, St. Louis, MO) were used as candidate antiscalants in this study. Hydrophobic PVDF membrane with a nominal pore size of 0.45 μm (Millipore Sigma, Burlington, MA) and BW30LE membranes (DuPont Filmtec, Edina, MN) were used in dynamic crossflow MD and RO experiments, respectively. Deionized (DI) water was produced from a commercial water purification system (>18 m Ω , Millipore, Burlington, MA).

2.2. Static experiments of silica polymerization

Y. Yao et al.

Static experiments were performed to evaluate the efficiencies of candidate antiscalants in hindering silicic acid polymerization. A silica-supersaturated solution consisting of 50 mM NaCl, 1 mM NaHCO₃, and 8 mM Na₂SiO₃·5H₂O (equivalent to 480 mg/L as SiO₂) was prepared. In this solution, the saturation index (SI, defined as the natural logarithm of the ratio between ion activity product and solubility equilibrium constant, $\frac{IAP}{K_{sp}}$) of silica was 0.66, as calculated by the PHREEQC software. For experimental groups with antiscalants, 40 mg/L of each candidate antiscalant was added to the silica-supersaturated solution. The solution pH was adjusted to 6.50 \pm 0.05 by using 1 M HCl and 0.5 M NaOH. The solution temperature was maintained at the room temperature (~21 °C).

The silicomolybdate method was used to quantify the concentrations of molybdate-reactive silica, which includes mono- and di-silicic acid (Preari et al., 2014), in the silica-supersaturated solution. The first seven samples were taken every 20 min within a period of 2 h, after which the samples were taken every 2 h. The total duration of the static experiment was 6 h. All samples were filtered by a 0.45 μm sterile syringe filter (VWR, Radnor, PA) before measurements. The concentration of molybdate-reactive silica was proportional to the absorbance at 420 nm measured by an ultraviolet—visible spectrophotometer (UV-1200, VWR, Radnor, PA). Additionally, the surface charge of silica particles formed at 6 h was measured using Zetasizer Nano ZS (Malvern Panaltyical, UK).

2.3. Dynamic MD silica scaling experiments

Dynamic silica scaling experiments were performed to evaluate the efficiencies of candidate antiscalants in reducing silica scaling in MD. The silica-supersaturated solutions (an initial volume of 1 L, pH of 6.50 \pm 0.05, temperature at 60 °C) for MD scaling experiments contained 8 mM Na₂SiO₃·5H₂O, 50 mM NaCl and 1 mM NaHCO₃, resulting in a SI of silica at 0.37. An additional 40 mg/L of antiscalant was added individually to the feedwater of the experimental groups. A custom-built, crossflow MD system was used with an effective membrane area of 20.02 cm² (Yin et al., 2021, 2022). The temperatures of the feed and distillate streams were maintained at 60 °C and 20 °C, which were circulated with crossflow velocities of 9.6 cm s $^{-1}$ and 6.4 cm s $^{-1}$, respectively. The water vapor flux, which was quantified by the weight change of the distillate reservoir, was monitored along the experiments. The membranes after the scaling experiments were air-dried and preserved for further investigation.

2.4. Dynamic RO silica scaling experiments

We also performed dynamic silica scaling experiments to evaluate the efficiencies of antiscalants in reducing silica scaling in RO. A custombuilt, crossflow RO system was used with an effective membrane area of $20.02~\text{cm}^2$ (Yin et al., 2022). The silica-supersaturated solutions (an initial volume of 5 L, pH of 6.50 ± 0.05) for RO scaling experiments contained 4 mM Na₂SiO₃·5H₂O, 50 mM NaCl and 1 mM NaHCO₃, resulting in an initial SI of silica at 0.35. A Lower concentration of silica was applied to RO experiments than that used in MD experiments because RO is typically used to treat feedwaters with lower salinities and antiscalant concentrations than MD (Tong and Elimelech, 2016; Yin

et al., 2022). An additional 20 mg/L of antiscalant was added individually to the feedwater of experimental groups, and the temperature was maintained at 22 \pm 1 °C. Such a concentration of antiscalant resulted in the same antiscalants/silicic acid ratio to those in the static experiments and dynamic MD experiments. The RO membrane was compacted overnight (using DI water as the feedwater) until the water flux did not change. The DI water was then replaced by the feed solutions that have been described above and a 24 h dynamic experiment was operated at a pressure of 450 \pm 10 psi to achieve an initial permeate flux of 45.0 \pm 0.5 L $m^{-2}\,h^{-1}$. The water flux was monitored along the experiment using a digital liquid flow meter (FlowCal 500, Tovatech, Plano, TX).

2.5. Silica scale characterization

Scanning electron microscopy (SEM, JEOL JSM-6500F, Peabody, MA) was employed to analyze the morphology of the silica scale formed on the MD and RO membrane surfaces. The surface chemical analysis was performed via X-ray photoelectron spectroscopy (XPS) with a PHI-5800 spectrometer (Physics Electronics, Chanhassen, MN) equipped with a monochromic Al-K X-ray sources, with the spectra calibration following the procedure described in our recent publication (Yin et al., 2021).

3. Results and discussion

3.1. Effects of antiscalants with different molecular structures on silicic acid polymerization

Fig. 2 presents the effects of different antiscalants on the polymerization of silicic acid during static experiments. In the absence of any antiscalants, the concentration of reactive silica (mainly mono- and disilicic acid (Preari et al., 2014)) decreased with time, resulting in a reduction from 480 mg/L (as SiO₂, the same for all the concentrations mentioned below) to 196 mg/L after 6 h. The presence of PEG slowed down the rate of silicic acid polymerization, with an increase of PEG MW generally leading to a better efficiency of silicic acid stabilization (Fig. 2A). Such a stabilizing effect became similar when the MW of PEG reached 6000, consistent with what was reported by Preari et al. (Preari et al., 2014). We also compared the performance of PEG with that of PEGD, which possesses a PEG backbone but is terminated with two amino groups (Fig. 1). As shown in Fig. 2B, PEGD10000 (i.e., PEGD with a MW of 10,000) exhibited an improved efficiency of stabilizing silicic acid than its PEG counterpart at the same MW, resulting in a 6 h concentration of molybdate-reactive silica at 389 mg/L that was higher than what was achieved with PEG10000 (350 mg/L). Although we acknowledge that the mechanism underlying the higher antiscaling efficiency of PEGD than PEG still needs to be fully elucided, we presumably attributes such a phenomenon to the change of polymer morphology by the terminal groups (Jo et al., 2013; Kim et al., 2020). The presence of terminal amino groups might alter the molecular conformation of PEGD in aqueous solutions compared to PEG, thereby changing the exposure of ethereal oxygens (the importance of ethereal oxgen to the efficiency of antiscalants will be explained below) to silicic acid and consequently the efficiency of hindering silic acid polymerization. For PEG, the terminal hydroxyl groups are able to form hydrogen bonding with each other and/or the ethereal group, forming an entangled PEG network (Begum and Hiroatsu Matsuura, 1997; Dormidontova, 2004) and/or reducing the available ethereal oxygens. In contrast, the protonated amine groups lead to electrostatic repulsion between the PEGD molecules, resulting in a more discrete but expened molucular conformation. The impact of molecular morphology could be also responsible for the effect of MW on antiscalant efficiency as shown in Fig. 2A (which will be discussed with more details below), as MW has been shown to alter molecular conformation of PEG in aqueous solutions (Nam et al., 2011).

The effects of antiscalants with other molecular functionalities on

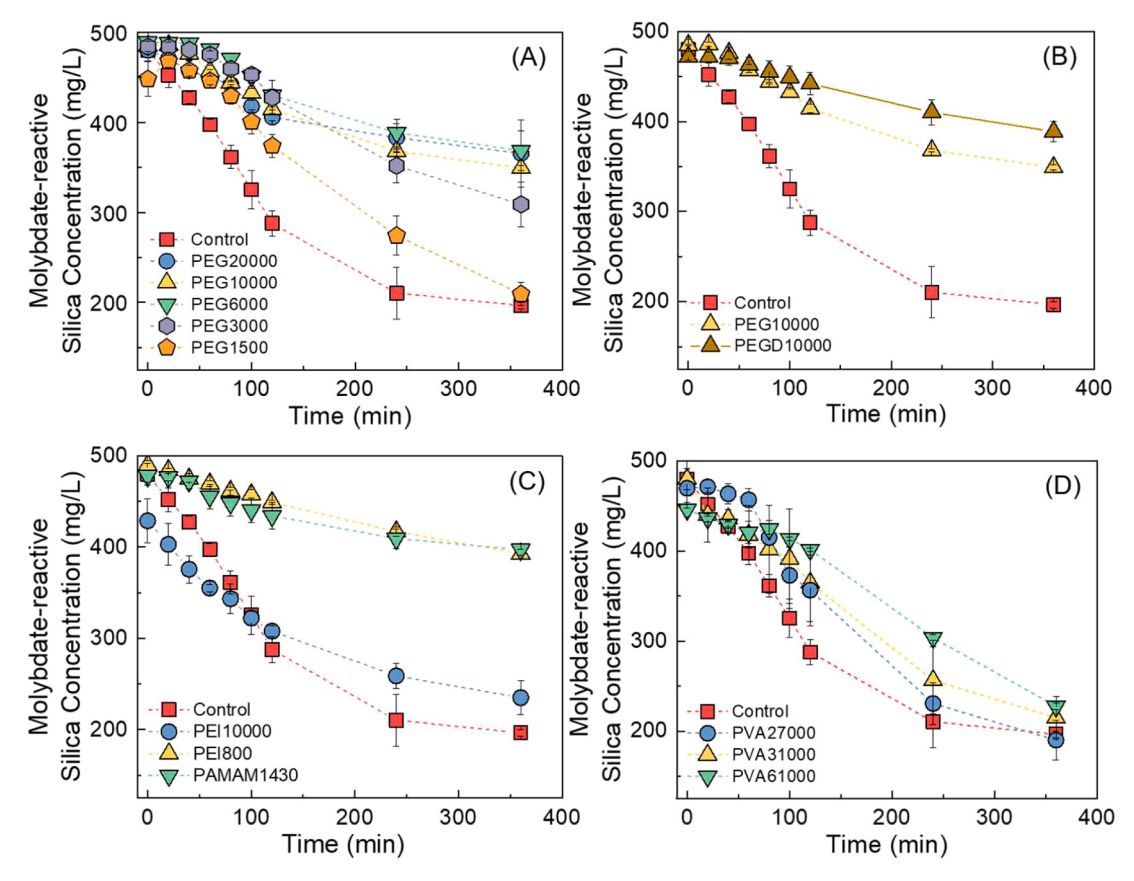


Fig. 2. The performance of silicic acid stabilization in static experiments by (A) PEG, (B) PEGD10000, (C) PEI800, PEI10000, and PAMAM1430, and (D) PVA. The concentrations of antiscalants were 40 mg/L in all experiments (pH of 6.50). The error bars represent standard deviations from three replicate experiments.

silicic acid polymerization were also investigated. As shown in Fig. 2C, PEI800 (i.e., PEI with a MW of 800) was able to stabilize 197 mg/L silica after 6 h, increasing the molybdate-reactive silica concentration to 393 mg/L. PAMAM1430 (i.e., PAMAM with a MW of 1430), another antiscalant possessing strong H-donors (e.g., primary and secondary amine groups), also demonstrated efficient antiscaling performance, resulting a similarly high molybdate-reactive silica concentration of 398 mg/L. However, the presence of PEI10000 (PEI with a MW of 10,000) resulted in a similarly rapid decrease of reactive silica concentration compared to the control group, indicating its lack of antiscaling efficiency. This suggests that different from PEG (for which the efficiency of antiscalant increased with MW), PEI with a higher MW led to a lower performance of stabilizing silicic acid. Furthermore, although PVA molecules, which possess functional groups as moderate H-donors (e.g., -OH), were able to decrease the rate of silicic acid polymerization (especially within the first 2 h, Fig. 2D), their stabilizing effects were moderate and much less significant than those of PEG, PEI, and PAMAM. Like what was observed for PEG, the efficiency of PVA for stabilizing silicic acid was enhanced when the MW of PVA molecules increased, but the overall efficiency of PVA was lower than other types of antiscalants tested in the current study. At the conclusion of the 6 h experiments, similar reactive silica concentrations were observed in the presence of PVA compared to the control group.

Our results demonstrate that the stabilizing effects of antiscalants on silicic acid polymerization are a function of both molecular functionality and weight. Interestingly, antiscalants enriched with strong H-accepters and H-donors (i.e., PEG, PEGD, and PEI800, PAMAM) were both able to hinder silicic acid polymerization efficiently in static experiments, with their antiscaling performance better than those with weaker capability of hydrogen bonding such as PVA. The formation of hydrogen bond has been suggested as the major mechanism for antiscalants that inhibit

silica polymerization (Kempter et al., 2013; Preari et al., 2014), and our results provide additional evidence to support the important role of hydrogen bonding in achieving the desired function of antiscalants for silica. The formation of silica proceeds either between two neutral silicic acid molecules or between ionized and neutral silicic acids (Greenberg and Sinclair, 1955). Regarding the former, the apex (-OH) of each silicic acid approaches each other and the polymerization reaction occurs between those adjacent silanol groups via the departure of a H₂O molecule (Garofalini and Martin, 1994). Regarding the latter, the deprotonated silanol group of the ionized silicic acid was suggested to form a temporary pentacoordinated Si (via a long Si-O bond) with a neutral silicic acid, which is followed by the departure of an -OH group that becomes an H₂O (Garofalini and Martin, 1994). The second mechanism has been shown to be faster and more favorable, controlling the rate of silicic acid polymerization (Fleming, 1986). The formation of hydrogen bonding between silicic acid and antiscalants could disrupt the interactions between silanol groups (e.g., preventing the formation of the long Si-O bond) and/or the departure of H₂O/-OH, thereby hindering the process of silicic acid polymerization.

We also noticed that the relationship between MW and the effect on silica polymerization differs among the antiscalants. Specifically, the hinderance of silica polymerization increased with MW for PEG and PVA, while it tended to decrease when the MW of PEI increased. We attribute such differences to the different silica-antiscalant interactions caused by different conformation. As we discussed above, the formation of hydrogen bonding between the antiscalants and silicic acid is likely to play an important role in determining the efficiency of antiscalant to hinder silica polymerization. Thus, the exposure of H-bond-forming functional groups, which is regulated by the conformation of the antiscalants in aqueous solutions, should be critical. As shown in the literature (de Lima et al., 2021; Kim et al., 2020; Yang et al., 2015), organic

polymers with different MWs exhibit varied conformations in aqueous solutions. The effect of MW on polymer conformation differs among different types of polymers because functional groups regulate inter- and intra-molecular interactions of the molecules. Further, as proposed by Iler (Iler, 1952), the ability of ether moieties to form hydrogen bonds exponentially increases with the number of ethylene oxide units connected in a single polymer chain, consistent with the increase of hindering effect with MW of PEG. However, similar relationships have not been reported for other polymers such as PEI.

In addition, the surface charge of silica particles formed in the absence and presence of representative antiscalants were quantified by measuring the zeta potential (Fig. 3). The presence of PEG, PEGD, and PVA, which possess functional groups that have lower deprotonation abilities than the silanol group (Bidlingmeyer et al., 1982; Farruggia et al., 1997; Hosny and Khalaf-Alaa, 2013), reduced the negative surface charge of silica particles. Also, the silica particles formed in the presence of PEGD were less negatively charged than those formed with PEG. Zeta potential measurements of PEG and PEGD molecules showed that the surface charge of those two polymers were both near neutral and not statistically different (Figure S1, Supplementary Materials). Therefore, the addition of two terminal amino groups did not alter the overall surface charge of PEG, and thus the less negative surface charge of silica particles with PEGD was likely resulted from the higher extent of coverage of silica surface by PEGD than PEG. Further, the presence of PEI and PAMAM reversed the surface charge of silica particles from negative to positive due to the abundant primary and secondary amine groups, which are protonated at near neutral pH (Gallops et al., 2020). The effects of different antiscalants on hindering silicic acid polymerization and the surface charge of silica particles are summarized in Table S1 (Supplementary Materials).

3.2. Efficiencies of antiscalants for mitigating silica scaling in membrane distillation

The performance of antiscalants shown in Fig. 2 to mitigate silica scaling was tested in dynamic MD experiments (Figs. 4 and S2, Supplementary Materials), in order to evaluate whether static antiscalant testing (which is typically performed when designing antiscalants (Demadis and Neofotistou, 2007; Neofotistou and Demadis, 2004; Preari et al., 2014)) is able to select effective antiscalants for practical MD applications. In the absence of antiscalants, the water vapor flux decreased sharply due to silica scaling when the water recovery of MD reached ~30% (Fig. 4). Despite their good efficiencies of stabilizing silicic acid in static antiscalant testing (for PEG with high MW), PEG was generally not effective to reduce silica scaling in MD, where only PEG20000 (i.e., PEG with a MW of 20,000, the highest MW of PEG in this study) was able to extend the water recovery from ~30% to ~60% (Figs. 4A and S2A). However, PEGD exhibited a much higher antiscaling efficiency than its PEG counterpart, with PEGD10000 (PEGD with the

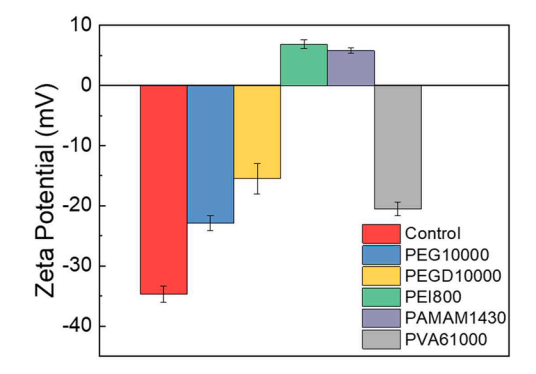


Fig. 3. Zeta potential of silica particles collected at 6 h from static experiments with different antiscalants.

highest MW that is commercially available by the vendor) extending the water recovery of MD to $\sim\!75\%$ (Figs. 4B and S2B). Further, both PEI800 and PAMAM1430, which showed high capabilities of stabilizing silicic acid in static antiscalant testing, effectively enhanced the water recovery of MD to $\sim\!80\%$ and $\sim\!70\%$, respectively (Figs. 4C and S2C). Coversely, PEI10000 with no antiscaling effects in static experiments resulted in an even faster water flux decline than the control group. This result could be due to the faster silicic acid polymerization induced by PEI10000 at the early stage of the experiments (Fig. 2C). In addition, PVA demonstrated limited efficiencies of reducing silica scaling in MD, similar to their moderate efficicacies of silicic acid stabilization as shown in Fig. 2D. Therefore, although the results of static antiscalant testing did not perfectly predict the performance of antiscalants in dynamic MD experiments, they generally identified potential antiscalants suitable for mitigating silica scaling in MD desalination.

The morphologies of silica scales formed on the PVDF membrane surfaces were characterized using SEM (Figs. 5). As shown in Fig. 5A, aggregates of silica particles with sizes of 100-200 nm were deposited into and covered the pores of PVDF membrane if no antiscalants were present. In the presence of PVA, no morphological changes were observed for silica scales (Fig. 5H). When PEG was present, compact, and seemingly impermeable gel layers were clearly found in addition to the deposition of silica particles (Fig. 5E). These gel layers were in accordance with the mechanism of silica scaling in MD as described in our previous publication (Yin et al., 2019): the water vapor flux decrease was due to the deposition of silica particles followed by the formation of a cross-linked, gel-like silica network via reactions of the deposited silica particles with the remaining silicic acid in the feed solution. However, such a gel layer of silica seemed to be absent when PEGD was added to the feed solution (Fig. 5G, with the silica scale layer being porous), explaining the better antiscaling performance of PEGD than PEG in MD (Fig. 4B). One possibility is that the higher extent of silica surface coverage by PEGD (as supported by the zeta potential results shown in Figs. 3 and S1) hindered the reaction of silica particles with the silicic acid in solution, disrupting the formation of the gel layer. Further, larger silica particles with more spherical shapes were observed when PAMAM1430 (Fig. 5B) and PEI800 (Fig. 5C) were applied to the feed solution, which were consistent with the findings of our previous study (Yin et al., 2021). The larger silica particles resulted in wider inter-particle space, requiring longer time to form the cross-linked gel layer that covers the membrane surface (i.e., longer induction time of water flux decline). However, the presence of PEI10000 resulted in the formation of a dense and impermeable scale layer consisting of smaller silica particles (than what was formed with PEI800). This result was in accordance with the lack of antiscaling efficiency of PEI10000. The results above indicate that antiscalant molecules with varied functionalities are able to control the morphology of silica formed in supersaturated aqueous solutions, analogous to the essential roles of organic molecules in regulating silica morphology in biomineralization (Kröger et al., 2000). Such roles pose an important effect on the silica-membrane interactions and the behaviors of MD desalination in the presence of antiscalants.

Furthermore, we performed XPS to explore the local chemical environment of Si for the scales formed on the membrane surface after MD scaling experiments by examining the high resolution Si 2p spectra (Fig. 6). When no antiscalants were added to the feed solution, a characteristic peak at 103.2 eV, which corresponds to the Si–O bond (Wagner et al., 1982), was observed. In the presence of PEG10000 and PEGD10000, the binding energies of Si 2p were shifted positively to 103.6 eV and 103.4 eV (Table S2, Supplementary Materials), respectively, indicating a decrease of electron density around the Si atoms. This was probably due to the formation of hydrogen bonding between silica and PEG/PEGD, in which PEG/PEGD behaved as H-accepters (via the ethereal oxygens). In contrast, the binding energy of Si 2p was shifted negatively to 102.9 eV and 102.4 eV in the presence of PEI800 and PAMAM1430 (Table S2), respectively, suggesting the increase of

Y. Yao et al. Water Research 246 (2023) 120701

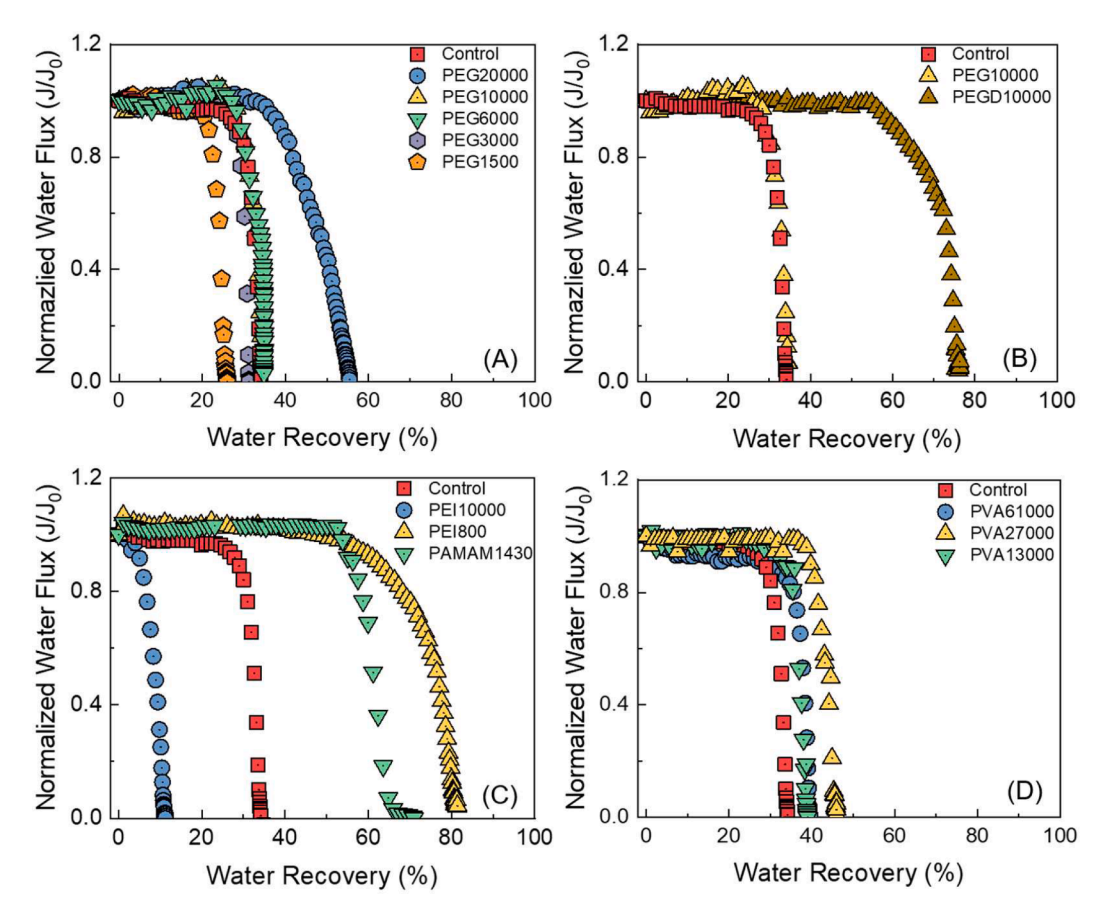


Fig. 4. Normalized water vapor flux as a function of water recovery ratio in dynamic MD silica scaling experiments with different antiscalants. The initial concentration of silica in the feed solutions was 8 mM and the concentrations of antiscalants were 40 mg/L in all experiments except for the control group. The temperatures of feed and permeate solutions were 60 °C and 20 °C, respectively. The feed and permeate streams were continuously circulated at crossflow velocities of 9.6 cm s⁻¹ and 6.4 cm s⁻¹, respectively. The initial water vapor flux of MD was 24.5 \pm 1 L m⁻² h⁻¹, which was used to normalize the water vapor fluxes. Replicate results are shown in Figure S2 of Supplementary Materials.

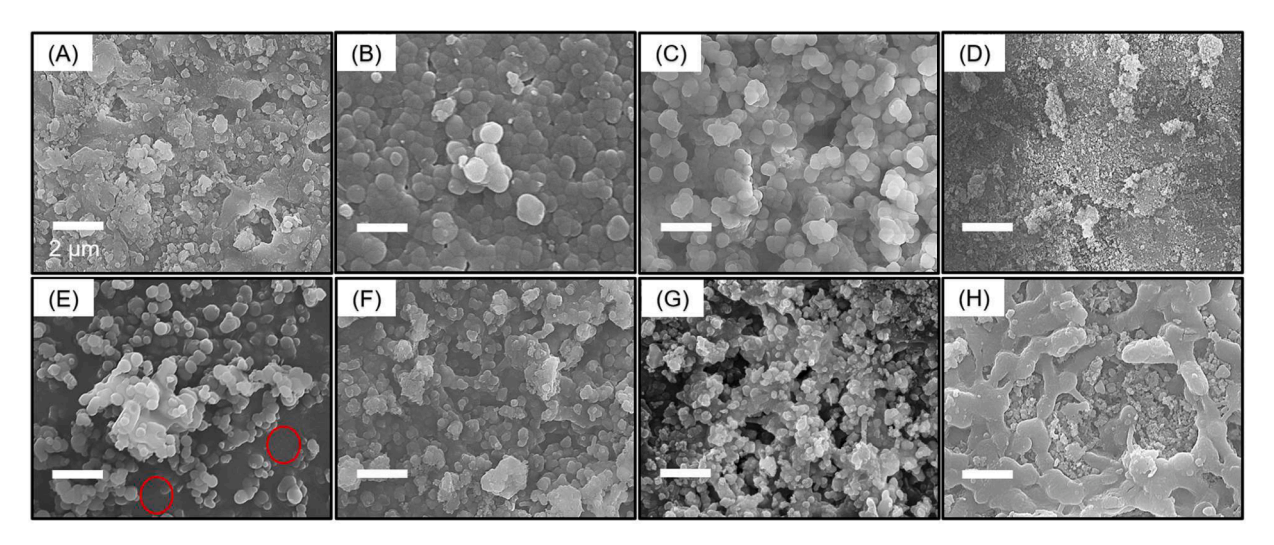


Fig. 5. SEM micrographs of PVDF membranes after dynamic MD silica scaling experiments (A) in the absence of any antiscalants and in the presence of (B) PAMAM1430, (C) PEI800, (D) PEI10000, (E) PEG10000, (F) PEG20000, (G) PEGD10000, and (H) PVA61000. The red circles point to silica gel layers on membrane surface. The magnifications of the micrographs are 10000X. The scale bars represent 2 μ m.

electron density around Si resulting from the H-donor nature of PEI and PAMAM. It is also worth mentioning that the extent of binding energy shift observed in our study is sufficient to indicate that alteration of local chemical environment of Si, as shown in the literature (Abada et al., 2022; Gao et al., 2018; Jia et al., 2015; Lu et al., 2023; Yin et al., 2021).

Also, the binding energy of Si 2p for silica precipitates formed in the presence of PVA was identical to what was observed for the control group, suggesting negligible chemical interactions between silica and PVA. This was due to the weaker capability of PVA to form hydrogen bonds and consistent with the more limited effects of PVA on silicic acid

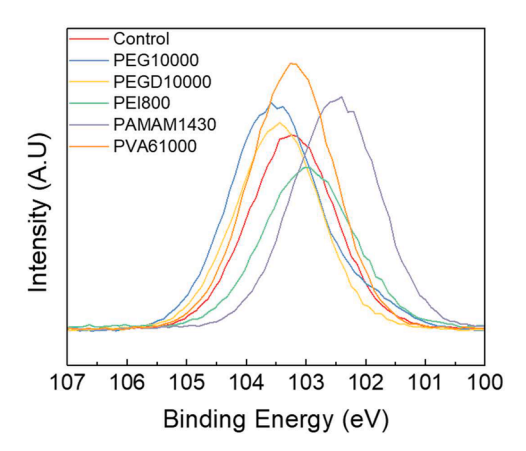


Fig. 6. High resolution XPS spectra of Si element for the silica scales formed on the PVDF membrane surface after MD scaling experiments. The peak positions indicating the Si 2p binding energy are summarized in Table S2 of Supplementary Materials.

polymerization (Fig. 2) and MD performance (Fig. 4) than other types of antiscalants. Thus, the XPS results provide additional evidence supporting that the antiscalants interact with silica via hydrogen bonding. Although beyond the scope of this work, liquid-state NMR spectroscopy, which directly analyzes silica-antiscalant interaction in aqueous solutions, and computational simulation (Garofalini and Martin, 1994; Rao and Gelb, 2004) have the potential of further elucidating the role of hydrogen bonding in the silica-antiscalant interactions and the consequent antiscalant efficiency.

3.3. Efficiencies of antiscalants for mitigating silica scaling in reverse osmosis

The performance of antiscalants that have shown promising antiscaling efficiencies during static testing and dynamic MD experiments was also probed in crossflow, dynamic RO experiments (Figs. 7 and S3, Supplementary Materials). As shown in Fig. 7, PEI800, which exhibited exceptional antiscaling efficacy in MD (Fig. 4), was unable to slow the rate of water flux decline caused by silica scaling in RO. Instead, it facilitated the decrease of water flux, especially during the intial phase of RO desalination. The difference in antiscaling efficacy of PEI800 bewteen RO and MD was due to the different working principles and

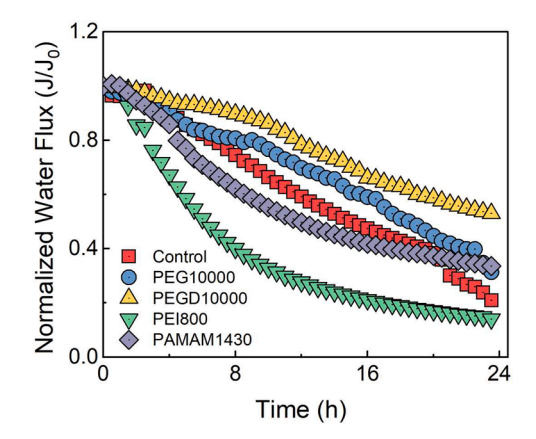


Fig. 7. Normalized water flux as a function of time in dynamic RO silica scaling experiments with different antiscalants. The initial concentration of silica was 4 mM and the concentrations of antiscalants were 20 mg/L in all experiments except for the control group. The operating pressure was 450 \pm 10 psi. The initial water vapor flux of RO was 45.0 \pm 0.5 L m^{-2} h^{-1} , which was used to normalize the water fluxes. Replicate results are shown in Figure S3 of Supplementary Materials.

silica scaling mechanisms associated with these two membrane processes. As we demonstrated in our previous work (Yin et al., 2019), the water vapor flux decline caused by silica scaling in MD was a result of homogeneous nucleation in the bulk solution followed by the deposition of silica particles and surface-mediated heterogeneous nucleation. Due to the micron-scale size of MD membrane pores, heterogeneous nucleation alone did not decrease water vapor flux significantly (Yin et al., 2019). In contrast, heterogeneous nucleation on membrane surface is the main mechanism that induces water flux decline in RO (Mi and Elimelech, 2013; Tong et al., 2017). As shown by Tong et al. and Lu et al. (Lu and Huang, 2019; Tong et al., 2017), less negatively charged membranes were subject to expedited water flux decrease caused by silica scaling in RO, due to the facilitated surface nucleation induced by a higher local concentration of negatively charged, reactive silica species near the membrane surface. The deposition of amine-abundant PEI800 to the membrane surface changed the membrane surface charge towards much less negative at near neutral pH (Figure S4, with experimental details in the Supplementary Materials) due to the positive charge carried by the primary and secondary amine groups, thereby promoting silica scaling. The presence of PEG10000 and PAMAM did not pose a significant impact on the water flux decrease induced by silica scaling (Figs. 7 and S3). The limited effect of PEG10000 on silica scaling in RO was similar to what was observed in MD experiments, despite of its high efficiency in static antiscalant testing. This result suggests again that static antiscalant testing is unable to perfectly predict the efficiency of antiscalants in dynamic membrane filtration. Further, PEI800 and PAMAM1430 are both enriched with amine groups as H-donors. Although PAMAM also facilitated the initial rate of flux decline caused by silica scaling in RO, its effect was much less significant than that of PEI800. As shown in Figure S4, the zeta potential of RO membrane exposed to PEI800 was much less negative than that of the control group (i.e., exposed to no antiscalants), whereas the presence of PAMAM1430 only slightly altered the membrane surface charge. Therefore, PAMAM1430 was less prone to attach to the polyamide RO membrane surface than PEI800, consequently posing a less profound effect on silica scaling. Furthermore, the best antiscaling efficacy was observed for PEGD10000, which increased the normalized water flux after 24 h significantly from ${\sim}0.2$ to ${\sim}0.5$. This result was consistent with the excellent efficiency of PEGD in hindering silicic acid polymerization as shown in Fig. 2.

We also performed SEM to observe the morphologies of silica scale formed on the polyamide RO membrane surface. A dense layer of silica particles was seen to fully cover the membrane surface without any antiscalant (Fig. 8A). Similar silica morphologies were observed when PEG10000 was present (Figs. 8B). The silica particles were larger when PEI800 or PAMAM1430 was present (Figs. 8D and E), consistent with what was observed on the MD membrane surface (Fig. 5). The sizes of silica particles formed in RO were generally smaller than those in MD, probably due to the different scale formation mechanisms between RO and MD processes. The most contrasting difference was observed when PEGD10000 was added to the feed solution: the density of silica particles on the membrane surface was lower than those on other membrane surfaces, with the texture of polyamide membrane surface being still visible (Fig. 8C). This result is consistent with the best antiscaling efficiency of PEGD10000 in RO.

4. Conclusion

In this work, we demonstrate that the efficiencies of antiscalants for silica scaling are a function of both molecular functionality and weight (as summarized in Table S1, Supplementary Materials). Although the interactions between silica and antiscalants are shown to be via hydrogen bonding, antiscalants behaving as strong H-accepters and strong H-donors are both able to effectively hinder silicic acid polymerization in static experiments, which have been typically used to identify antiscalants for silica scaling (Demadis, 2008; Demadis et al.,

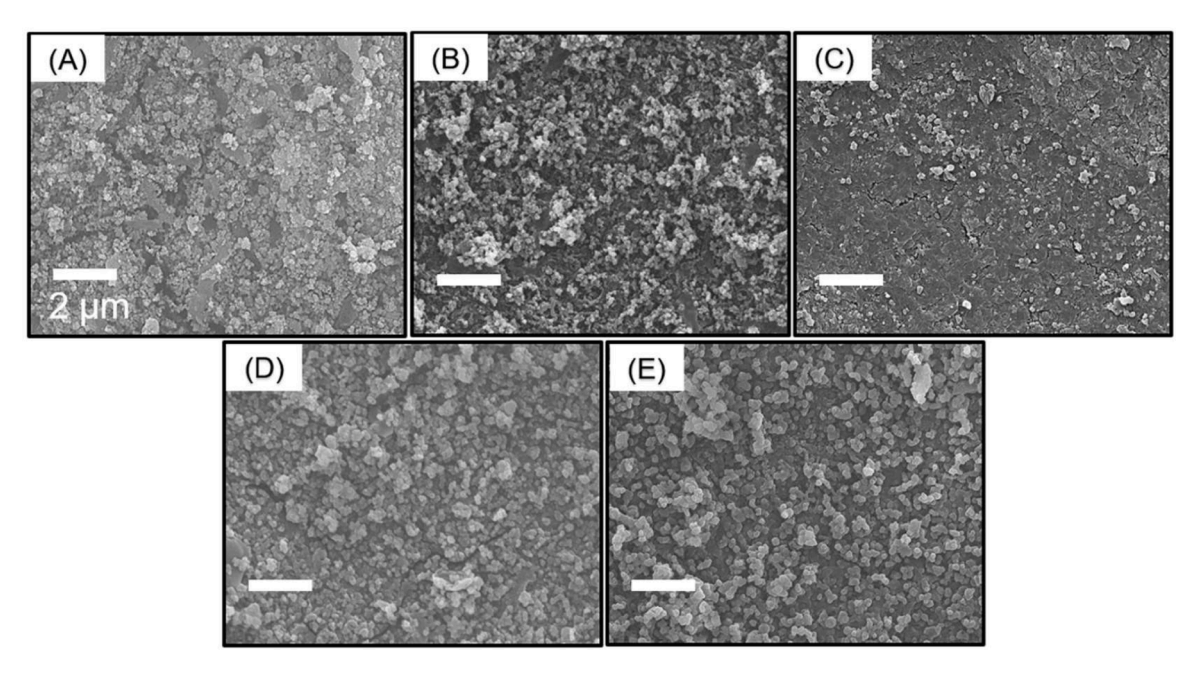


Fig. 8. SEM micrographs of the BW30LE membranes after dynamic RO silica scaling experiments: (A) in the absence of any antiscalants and in the presence of (B) PEG10000, (C) PEGD10000, (D) PEI800 and (E) PAMAM1430. The magnifications of the micrographs are 10000X. The scale bars present 2 μm.

2005; Neofotistou and Demadis, 2004; Preari et al., 2014). As antiscalants with different molecular weights and terminal groups exhibited varied antiscaling efficiencies, the conformation of the antiscalant molecules in aqueous solution is likely to play an important role in governing the interactions of antiscalants with silicic acid. However, we admit that such a hypothesis has yet to be validated, due to the tremedous work needed to investigate the molecular conformation of antiscalants and its effects on silica-antiscalant interactions. This warrants future work to consider molecular conformation in the structure-property-performance relationship of antiscalants for silica scaling.

Further, the results from static experiments were able to generally (but not perfectly) identify effective antiscalants for dynamic MD experiments, but they were unable to predict how antiscalants behaved in dynamic RO experiments, highlighting the difference in silica scaling mechanisms between these two membrane processes. In MD, homogeneous nucleation of minerals in the bulk solution is more prone to occur than RO due to the higher salt and scalant concentrations of the feedwater. The water vapor flux decline caused by silica scaling in MD is caused by the formation of a cross-linked silica gel layer, which results from homogeneous nucleation followed by silica particle deposition and surface nucleation (Yin et al., 2019). As a result, the efficiency of antiscalants in MD is relevant to their effects of hindering silicic acid polymerization in aqueous solutions (i.e., as manifested by results of static experiments) and altering silica morphology (to disrupt the formation of silica gel layer). In RO, however, the more important role of heterogenous nucleation on the membrane surface in directly inducing water flux decline scaling renders the efficiencies of antiscalants be regulated by not only their efficacy of hindering silicic acid polymerization but also their effects on altering membrane surface property. For antiscalants with abundant functional groups as H-donors, which are positively charged at the near neutral pH, the attachment of antiscalants to the membrane surface shifted the membrane surface charge towards less negative, facilitating silica scaling by attracting the negatively charged, reactive silica species (Tong et al., 2017). As a result, although antiscalants like PEI800 and PAMAM1430 were able to successfully extend the water recovery of MD in the presence of silica scaling, they were ineffective in RO and conversely facilitated the decrease of water flux. Successful antiscalants for silica scaling in RO should be effective of hindering silicic acid polymerization in static experiments meanwhile avoiding carrying abundant functional groups as H-donors. Therefore, our results indicate that the design of antiscalants for silica scaling needs to be tailored to specific membrane processes.

Last, but not least, we showed that PEGD10000 were an effective antiscalants in both MD and RO, but more work is required to fully understand the higher antiscaling efficiency of PEGD compared to PEG. It is challenging to explore the interactions between antiscalants and silicic acid in aqueous solutions experimentally, and thus computational approaches such as molecular dynamics simulation (Brückner et al., 2016; Garofalini and Martin, 1994) could be applied as a powerful tool to further close this knowledge gap. Additionally, exploring more antiscalants with similar but well-controlled, slightly differed structures and functionalities (e.g., sharing the same backbone but with different types or numbers of terminal groups) will provide more insights to further establish the structure-property-performance relationship of antiscalants for silica scaling.

Declaration of Competing Interest

The authors declare the following financial interests/personal relationships which may be considered as potential competing interests: Tiezheng Tong has patent Antiscalants for Mitigating Silica Scaling in Membrane Desalination pending to Colorado State University. Yiqun Yao has patent Antiscalants for Mitigating Silica Scaling in Membrane Desalination pending to Colorado State University. Yiming Yin has patent Antiscalants for Mitigating Silica Scaling in Membrane Desalination pending to Colorado State University.

Data availability

Data will be made available on request.

Acknowledgement

This material is based upon work supported by the National Science Foundation under Grant No. 2145627. Any opinions, findings, and conclusions or recommendations expressed in this material are those of Y. Yao et al. Water Research 246 (2023) 120701

the author(s) and do not necessarily reflect the views of the National Science Foundation.

Supplementary materials

Supplementary material associated with this article can be found, in the online version, at doi:10.1016/j.watres.2023.120701.

References

- Abada, B., Safarik, J., Ishida, K.P., Chellam, S., 2022. Surface characterization of end-of-life reverse osmosis membranes from a full-scale advanced water reuse facility: Combined role of bioorganic materials and silicon on chemically irreversible fouling. Journal of Membrane Science 653, 120511.
- Atia, A.A., Yip, N.Y., Fthenakis, V., 2021. Pathways for minimal and zero liquid discharge with enhanced reverse osmosis technologies: Module-scale modeling and techno-economic assessment. Desalination 509, 115069.
- Begum, R., Hiroatsu Matsuura, A., 1997. Conformational properties of short poly (oxyethylene) chains in water studied by IR spectroscopy. Journal of the Chemical Society, Faraday Transactions 93 (21), 3839–3848.
- Bidlingmeyer, B.A., Del Rios, J.K., Korpi, J., 1982. Separation of organic amine compounds on silica gel with reversed-phase eluents. Analytical Chemistry 54 (3), 442–447.
- Brückner, S.I., Donets, S., Dianat, A., Bobeth, M., Gutiérrez, R., Cuniberti, G., Brunner, E., 2016. Probing Silica–Biomolecule Interactions by Solid-State NMR and Molecular Dynamics Simulations. Langmuir 32 (44), 11698–11705.
- Charcosset, C., 2009. A review of membrane processes and renewable energies for desalination. Desalination 245 (1), 214–231.
- Chaussemier, M., Pourmohtasham, E., Gelus, D., Pécoul, N., Perrot, H., Lédion, J., Cheap-Charpentier, H., Horner, O., 2015. State of art of natural inhibitors of calcium carbonate scaling. A review article. Desalination 356, 47–55.
- de Lima, B.M., Hayes, P.L., Wood-Adams, P.M., 2021. Influence of Polymer Molecular Weight on Chain Conformation at the Polystyrene/Silver Interface. Langmuir 37 (33), 10036–10045.
- Demadis, K.D. 2008 Silica Scale Inhibition Relevant to Desalination Technologies: Progress and Recent Developments.
- Demadis, K.D., Neofotistou, E., 2007. Synergistic Effects of Combinations of Cationic Polyaminoamide Dendrimers/Anionic Polyelectrolytes on Amorphous Silica Formation: A Bioinspired Approach. Chemistry of Materials 19 (3), 581–587.
- Demadis, K.D., Neofotistou, E., Mavredaki, E., Tsiknakis, M., Sarigiannidou, E.M., Katarachia, S.D., 2005. Inorganic foulants in membrane systems: chemical control strategies and the contribution of "green chemistry. Desalination 179 (1), 281–295.
- Deshmukh, A., Boo, C., Karanikola, V., Lin, S., Straub, A.P., Tong, T., Warsinger, D.M., Elimelech, M., 2018. Membrane distillation at the water-energy nexus: limits, opportunities, and challenges. Energy & Environmental Science 11 (5), 1177–1196.
- Dormidontova, E.E., 2004. Influence of End Groups on Phase Behavior and Properties of PEO in Aqueous Solutions. Macromolecules 37 (20), 7747–7761.
- Elimelech, M., Phillip, W.A., 2011. The Future of Seawater Desalination: Energy, Technology, and the Environment. Science 333 (6043), 712–717.
- Farruggia, B., Garcia, G., D'Angelo, C., Picó, G., 1997. Destabilization of human serum albumin by polyethylene glycols studied by thermodynamical equilibrium and kinetic approaches. International Journal of Biological Macromolecules 20 (1), 43-51
- Fleming, B.A., 1986. Kinetics of reaction between silicic acid and amorphous silica surfaces in NaCl solutions. Journal of Colloid and Interface Science 110 (1), 40–64.
- Gallops, C., Ziebarth, J., Wang, Y., 2020. Polymers in Therapeutic Delivery. American Chemical Society, pp. 1-12.
- Gao, X., Yan, R., Xu, L., Ma, H., 2018. Effect of amorphous phytic acid nanoparticles on the corrosion mitigation performance and stability of sol-gel coatings on cold-rolled steel substrates. Journal of Alloys and Compounds 747, 747–754.
- Garofalini, S.H., Martin, G., 1994. Molecular Simulations of the Polymerization of Silicic Acid Molecules and Network Formation. The Journal of Physical Chemistry 98 (4), 1311–1316.
- Grant, S.B., Saphores, J.D., Feldman, D.L., Hamilton, A.J., Fletcher, T.D., Cook, P.L.M., Stewardson, M., Sanders, B.F., Levin, L.A., Ambrose, R.F., Deletic, A., Brown, R., Jiang, S.C., Rosso, D., Cooper, W.J., Marusic, I., 2012. Taking the "Waste" Out of "Wastewater" for Human Water Security and Ecosystem Sustainability. Science 337 (6095), 681–686.
- Greenberg, S.A., Sinclair, D., 1955. The Polymerization of Silicic Acid. The Journal of Physical Chemistry 59 (5), 435–440.
- He, F., Sirkar, K.K., Gilron, J., 2009. Effects of antiscalants to mitigate membrane scaling by direct contact membrane distillation. Journal of Membrane Science 345 (1), 53–58.
- Hoekstra, A.Y., 2014. Water scarcity challenges to business. Nat Clim Change 4 (5), 318-320.
- Hosny, W.M., Khalaf-Alaa, P.A., 2013. Potentiometric Study and Biological Activity of Some Metal Ion Complexes of Polyvinyl Alcohol (PVA). International Journal of Electrochemical Science 8 (1), 1520–1533.
- Iler, R.K., 1952. Association between Polysilicic Acid and Polar Organic Compounds. The Journal of Physical Chemistry 56 (6), 673–677.
- Jia, Y., Chen, L., Feng, X., Zhou, H., Chen, J., 2015. Tribological behavior of molybdenum disulfide bonded solid lubricating coatings cured with organosiloxanemodified phosphate binder. RSC Advances 5 (85), 69606–69615.

Jo, G., Ahn, H., Park, M.J., 2013. Simple Route for Tuning the Morphology and Conductivity of Polymer Electrolytes: One End Functional Group is Enough. ACS Macro Letters 2 (11), 990–995.

- Kempter, A., Gaedt, T., Boyko, V., Nied, S., Hirsch, K., 2013. New insights into silica scaling on RO-membranes. Desalination and Water Treatment 51 (4-6), 899–907.
- Kim, J., Jung, H.Y., Park, M.J., 2020. End-Group Chemistry and Junction Chemistry in Polymer Science: Past, Present, and Future. Macromolecules 53 (3), 746–763.
- Kröger, N., Deutzmann, R., Bergsdorf, C., Sumper, M., 2000. Species-specific polyamines from diatoms control silica morphology. Proceedings of the National Academy of Sciences 97 (26), 14133–14138.
- Lu, K.G., Huang, H., 2019. Dependence of initial silica scaling on the surface physicochemical properties of reverse osmosis membranes during bench-scale brackish water desalination. Water Research 150, 358–367.
- Lu, K.G., Ma, S., Hua, D., Liu, H., Li, C., Song, J., Huang, H., Qin, Y., 2023. Silica mitigated calcium mineral scaling in brackish water reverse osmosis. Water Research 243, 120428.
- Lu, X., Elimelech, M., 2021. Fabrication of desalination membranes by interfacial polymerization: history, current efforts, and future directions. Chemical Society Reviews 50 (11), 6290–6307.
- Malmsten, M., Linse, P., Cosgrove, T., 1992. Adsorption of PEO-PPO-PEO block copolymers at silica. Macromolecules 25 (9), 2474–2481.
- Mi, B., Elimelech, M., 2013. Silica scaling and scaling reversibility in forward osmosis. Desalination 312, 75–81.
- Mizutani, T., Nagase, H., Fujiwara, N., Ogoshi, H., 1998. Silicic Acid Polymerization Catalyzed by Amines and Polyamines. Bulletin of the Chemical Society of Japan 71 (8), 2017–2022.
- Nam, S., Parikh, D.V., Condon, B.D., Zhao, Q., Yoshioka-Tarver, M., 2011. Importance of poly(ethylene glycol) conformation for the synthesis of silver nanoparticles in aqueous solution. Journal of Nanoparticle Research 13 (9), 3755–3764.
- Neofotistou, E., Demadis, K.D., 2004. Use of antiscalants for mitigation of silica (SiO2) fouling and deposition: fundamentals and applications in desalination systems. Desalination 167, 257–272.
- Pike, S.J., Lavagnini, E., Varley, L.M., Cook, J.L., Hunter, C.A., 2019. H-Bond donor parameters for cations. Chemical Science 10 (23), 5943–5951.
- Preari, M., Spinde, K., Lazic, J., Brunner, E., Demadis, K.D., 2014. Bioinspired Insights into Silicic Acid Stabilization Mechanisms: The Dominant Role of Polyethylene Glycol-Induced Hydrogen Bonding. Journal of the American Chemical Society 136 (11), 4236–4244.
- Rao, N.Z., Gelb, L.D., 2004. Molecular Dynamics Simulations of the Polymerization of Aqueous Silicic Acid and Analysis of the Effects of Concentration on Silica Polymorph Distributions, Growth Mechanisms, and Reaction Kinetics. The Journal of Physical Chemistry B 108 (33), 12418–12428.
- Reiss, A.G., Gavrieli, I., Ganor, J., 2020. The effect of phosphonate-based antiscalant on gypsum precipitation kinetics and habit in hyper-saline solutions: An experimental and modeling approach to the planned Red Sea – Dead Sea Project. Desalination 496, 114638.
- Rolf, J., Cao, T., Huang, X., Boo, C., Li, Q., Elimelech, M., 2022. Inorganic Scaling in Membrane Desalination: Models, Mechanisms, and Characterization Methods. Environmental Science & Technology 56 (12), 7484–7511.
- Rubio, J., Kitchener, J.A., 1976. The mechanism of adsorption of poly(ethylene oxide) flocculant on silica. Journal of Colloid and Interface Science 57 (1), 132–142.
- Shaffer, D.L., Arias Chavez, L.H., Ben-Sasson, M., Romero-Vargas Castrillón, S., Yip, N.Y., Elimelech, M., 2013. Desalination and Reuse of High-Salinity Shale Gas Produced Water: Drivers, Technologies, and Future Directions. Environmental Science & Technology 47 (17), 9569–9583.
- Tong, T., Carlson, K.H., Robbins, C.A., Zhang, Z., Du, X., 2019a. Membrane-based treatment of shale oil and gas wastewater: The current state of knowledge. Frontiers of Environmental Science & Engineering 13 (4).
- Tong, T., Elimelech, M., 2016. The Global Rise of Zero Liquid Discharge for Wastewater Management: Drivers, Technologies, and Future Directions. Environmental Science & Technology 50 (13), 6846–6855.
- Tong, T., Wallace, A.F., Zhao, S., Wang, Z., 2019b. Mineral scaling in membrane desalination: Mechanisms, mitigation strategies, and feasibility of scaling-resistant membranes. Journal of Membrane Science 579, 52–69.
- Tong, T., Zhao, S., Boo, C., Hashmi, S.M., Elimelech, M., 2017. Relating Silica Scaling in Reverse Osmosis to Membrane Surface Properties. Environmental Science & Technology 51 (8), 4396–4406.
- Turek, M., Mitko, K., Piotrowski, K., Dydo, P., Laskowska, E., Jakóbik-Kolon, A., 2017.
 Prospects for high water recovery membrane desalination. Desalination 401, 180–189.
- Vörösmarty, C.J., McIntyre, P.B., Gessner, M.O., Dudgeon, D., Prusevich, A., Green, P., Glidden, S., Bunn, S.E., Sullivan, C.A., Liermann, C.R., Davies, P.M., 2010. Global threats to human water security and river biodiversity. Nature 467 (7315), 555–561.
- Wagner, C.D., Passoja, D.E., Hillery, H.F., Kinisky, T.G., Six, H.A., Jansen, W.T., Taylor, J.A., 1982. Auger and Photoelectron Line Energy Relationships in Aluminum-Oxygen and Silicon-Oxygen Compounds. J Vac Sci Technol 21 (4), 933–944.
- Wallace, A.F., DeYoreo, J.J., Dove, P.M., 2009. Kinetics of Silica Nucleation on Carboxyland Amine-Terminated Surfaces: Insights for Biomineralization. Journal of the American Chemical Society 131 (14), 5244–5250.
- Warsinger, D.M., Swaminathan, J., Guillen-Burrieza, E., Arafat, H.A., Lienhard, V, J.H., 2015. Scaling and fouling in membrane distillation for desalination applications: A review. Desalination 356, 294–313.
- Yang, S., Liu, Z., Liu, Y., Jiao, Y., 2015. Effect of molecular weight on conformational changes of PEO: an infrared spectroscopic analysis. Journal of Materials Science 50 (4), 1544–1552.

Y. Yao et al. Water Research 246 (2023) 120701

- Yin, Y., Jeong, N., Minjarez, R., Robbins, C.A., Carlson, K.H., Tong, T., 2021. Contrasting Behaviors between Gypsum and Silica Scaling in the Presence of Antiscalants during Membrane Distillation. Environmental Science & Technology 55 (8), 5335–5346.
- Yin, Y., Kalam, S., Livingston, J.L., Minjarez, R., Lee, J., Lin, S., Tong, T., 2022. The use of anti-scalants in gypsum scaling mitigation: Comparison with membrane surface modification and efficiency in combined reverse osmosis and membrane distillation. Journal of Membrane Science 643, 120077.
- Yin, Y., Wang, W., Kota, A.K., Zhao, S., Tong, T., 2019. Elucidating mechanisms of silica scaling in membrane distillation: effects of membrane surface wettability. Environmental Science: Water Research & Technology 5 (11), 2004–2014.
- Yu, W., Song, D., Chen, W., Yang, H., 2020. Antiscalants in RO membrane scaling control. Water Research 183, 115985.